Pharm Res (2014) 31:2220–2233
DOI 10.1007/s11095-014-1320-8

RESEARCH PAPER

Targeted Paclitaxel Delivery to Tumors Using Cleavable PEG-Conjugated Solid Lipid Nanoparticles

Jie Zheng • Yu Wan • Abdelbary Elhissi • Zhirong Zhang • Xun Sun

Received: 12 September 2013 / Accepted: 28 January 2014 / Published online: 5 March 2014

ABSTRACT

Purpose To develop a tumor-targeted drug delivery system based on solid lipid nanoparticles (SLNs) conjugated with the enzymatically cleavable polyethylene glycol (PEG).

Methods SLNs loaded with paclitaxel (PTX) were prepared using the film ultrasonication method, followed by conjugation with a PEGylated peptide (Pp) that can specifically interact with matrix metalloproteinases (MMPs) that is over-expressed by tumor cells. The physicochemical characteristics of the Pp-PTX-SLNs were studied and the *in vitro* drug release, cytotoxicity and cell uptake of the formulations were investigated. Furthermore, using an animal model, the pharmacokinetic properties, biodistribution and anti-tumor activity of this system were evaluated.

Results The resulting Pp-PTX-SLNs penetrated through tumor cells via facilitated uptake mediated by MMPs. The uncleavable Pp'-PTX-SLNs showed a lower cell uptake efficiency, compared with the Pp-PTX-SLNs. In a tumor-bearing mice model, Pp-PTX-SLNs accumulated to a greater extent at the tumor location, persisted longer in blood circulation, and showed lower toxicity than did PTX-SLNs or Taxol®. Most importantly, the mice treated with Pp-PTX-SLNs survived longer than the groups treated with Pp'-PTX-SLNs, PTX-SLNs or Taxol®.

Conclusions These results suggest that Pp-PTX-SLNs hold promise as a new strategy for paclitaxel chemotherapy, and that Pp-SLNs can be a useful nanocarrier for other chemotherapeutic drugs.

KEY WORDS MMP · paclitaxel · PEG · solid lipid nanoparticles · targeted therapy

ABBREVIATIONS

CE	Conjugation efficiency
CHO cells	Chinese hamster ovary cells
DL%	Drug loading
EE%	Encapsulation efficiency
EPR	Enhanced permeability and retention
GMS	Glyceryl monostearate
HT1080 cells	Human fibrosarcoma cells
LLC cells	Lewis lung carcinoma cells
MCT	Medium-chain triglycerides
MMP	Matrix metalloproteinase
OA	Octadecylamine
PEG	Polyethylene glycol
Pp	PEG2000-MMP substrate peptide (PEG2000-Gly-Pro-Leu-Gly-Ile-Ala-Gly-Gln-Cys)
Pp'	PEG2000-Ile-Pro-Gly-Gln-Gly-Ala-Leu-Gly-Cys
PTX	Paclitaxel
RES	Reticuloendothelial system
SLNs	Solid lipid nanoparticles
SPC	Soya phosphatidyl choline

Electronic supplementary material The online version of this article (doi:10.1007/s11095-014-1320-8) contains supplementary material, which is available to authorized users.

J. Zheng • Y. Wan • Z. Zhang • X. Sun
Key Laboratory of Drug Targeting and Drug Delivery Systems
Ministry of Education, West China School of Pharmacy, Sichuan University
Chengdu 610041, China

A. Elhissi
Institute of Nanotechnology and Bioengineering
School of Pharmacy and Biomedical Sciences
University of Central Lancashire
Preston PR1 2HE, UK

X. Sun (✉)
West China School of Pharmacy, Sichuan University
Chengdu 610041, China
e-mail: xunsun22@gmail.com

INTRODUCTION

Paclitaxel (PTX), one of the most effective chemotherapeutic drugs, plays a crucial role in the treatment of numerous cancers, such as ovarian and breast cancer, non-small cell lung carcinoma, melanoma, head and neck cancer, and AIDS-related cancer (1,2). However, the poor water-solubility of PTX (<0.1 μg/ml) is a serious limitation (3), hence extensive research has been conducted to find suitable vehicles for this drug. A clinically approved formulation of PTX is Taxol® consists of the drug dissolved in a mixture of Cremophor EL® (polyethoxylated castor oil) and dehydrated ethanol (1:1). Cremophor EL® is a very good solubilizer for PTX, however, it is known to cause many adverse effects, including severe hypersensitivity reactions, nephrotoxicity, neutropenia and neurotoxicity (4). Therefore, developing a Cremophor®-free formulation of PTX is essential for reducing the toxicity of the formulation. As a result, Abraxane®, an injectable suspension of albumin-bound paclitaxel has been developed and recently approved by the U.S. Food and Drug Administration. However, human albumin is difficult to obtain in large quantities, resulting in increased cost of this product. Thus, there is a need to develop PTX formulations that are safe, effective and economically affordable.

Many PTX delivery systems have been introduced such as liposomes (5), micelles (6), emulsions (7) and solid lipid nanoparticles (SLNs) (8). Amongst these systems, SLNs have attracted particular attention because of their high aqueous solubility, controlled release, physical stability, inexpensive large-scale production and low toxicity *in vivo* (9). On one hand, SLNs, like other nanocarriers, can accumulate at tumor sites via the enhanced permeability and retention (EPR) effect. On the other hand, SLNs present a major challenge because they are rapidly cleared via phagocytosis by the reticuloendothelial system (RES) and the mononuclear phagocytic system. Thus, designing SLNs that can circulate for longer periods *in vivo* and that can be targeted to tumor sites and internalized into cancer cells is a considerable challenge.

One successful approach for preventing nanoparticle uptake by macrophages is to attach flexible, hydrophilic polyethylene glycol (PEG) molecules to the nanoparticle surface. The presence of PEG prolongs nanoparticle circulation time and increases nanoparticle accumulation at the tumor tissues(10). However, PEGylation inhibits nanoparticle uptake into cells and negatively affects intracellular trafficking of the nanoparticles (11), significantly reducing drug delivery efficacy. This highlights the need for reversible PEGylation in which PEG would coat the nanocarrier for a period of time that is long enough for targeting to the tumor cells, after which the nanoparticles are "de-PEGylated" to be efficiently taken up by the cancer cells.

Recent approaches for de-PEGylation involve the use of pH and temperature-sensitive PEGylation (12), resulting in detachment of PEG molecules from the nanocarrier surface in the tumor microenvironment. A more specific and sensitive approach is to use PEG that can be cleaved by tumor-specific enzymes (13). Matrix metalloproteinase (MMP) is an overexpressed enzyme involved in the angiogenesis, invasion and metastasis of malignant tumors, as reported in several preclinical and clinical studies of melanoma (14,15). Recently, our group (16) described a lipid material cleaved by MMP-2. Specifically, we modified liposomes with PEGylated MMP-2 substrate and found that tumor-overexpressed MMPs cleaved the peptide bonds and effectively detached the PEG chains. Hence, modifying nanoparticles with MMP-cleavable PEG may result in efficient and selective targeting of SLNs to tumors. In this study, a PTX drug delivery system based on SLNs conjugated with PEG_{2000}-MMP substrate peptide (Pp) was developed.

MATERIALS AND METHODS

Materials

PEG_{2000}-Gly-Pro-Leu-Gly-Ile-Ala-Gly-Gln-Cys (Pp), and PEG_{2000}-Ile-Pro-Gly-Gln-Gly-Ala-Leu-Gly-Cys (Pp') (the former peptide is specific to MMP, while the latter one is non-specific) were custom-synthesized by Apeptides (Shanghai, China). Soya phosphatidyl choline (SPC) was purchased from Lipoid (Ludwigshafen, Germany). Octadecylamine (OA) was obtained from Bio Basic (Shanghai, China). Glyceryl monostearate (GMS) was purchased from Sigma (St Louis, MO, USA). Paclitaxel was purchased from HaoXuan Biological Technology Company (Xi'an, China, purity > 99%) and Taxol® was purchased from TaiJi Industry (Chongqing, China). The reagents 1-ethyl-3-(3-dimethylamino)propylcarbodiimide hydrochloride (EDC·HCl) and N-hydroxysuccinimide (NHS) were purchased from Best Reagent Company (Chengdu, China).

Dulbecco's Modified Eagle Medium (high glucose) (DMEM-HG) and penicillin-streptomycin mixture were obtained from Hyclone (Shanghai, China). Fetal bovine serum was purchased from Fumeng Gene (Shanghai, China), and Tyrisin was supplied by GIBCO (USA). 3-(4,5-methylthiazol-2-yl)-2,5-diphenyltetrazolium bromide (MTT) was obtained from Amresco (Solon, Ohio, USA). Coomassie (Bradford) protein assay was supplied by Bio Sharp (Shanghai, China), and the BCA protein assay kit was purchased from Thermo Scientific Pierce (Rockford, USA). Coumarin-6 was purchased from Sigma (purity >98%). All chemicals and solvents used in this study were of analytical grade.

Identification of MMP Activity in Tumor Cells

Cell Culture

Human fibrosarcoma cells (HT1080), Lewis lung carcinomacells (LLC) and Chinese hamster ovary cells (CHO) were obtained

from the Shanghai Cell Institute of the Chinese Academy of Sciences. The cells were cultured in complete DMEM-HG medium supplemented with 10% (v/v) fetal bovine serum (FBS), penicillin (100 U/mL) and streptomycin (100 μg/mL). Cells were maintained in a SANYO incubator at 37°C in a 5% CO_2 atmosphere.

Concentration of MMPs in Tumor Cell Supernatants

Once cells had reached the logarithmic phase of growth, the culture medium was replaced with non-FBS DMEM-HG and cells were incubated for another 48 h. Then the cell supernatants were assembled and centrifuged at 2,600 g for 10 min to obtain clarified supernatants which were then injected through 0.22 μm filters to remove residual cell debris and microorganisms. The supernatant was concentrated to approximately 250 μL using the Amicon®Ultra-15 30 K Centrifugal Filter Devices (Millipore, USA) at 4,000 g for 15 min.

Gelatin Zymography Assay

To evaluate whether the concentrated cell supernatants contained MMP-2, gelatin zymography was performed as described in our previous study (16). Briefly, the cell supernatants of HT1080 and LLC, as well as purified MMP-2 (as a positive control), were injected into the gel wells. After electrophoresis, the gel was immersed in a buffer system containing divalent metal ions to reactivate MMPs that might be present in the samples. The partially renatured enzymes can hydrolyze the gelatin, leaving a cleared zone that can be detected after staining of the gel with Coomassie Brilliant Blue R-250. The degree of gelatin degradation is proportional to the amount of MMP-2 contained in the sample.

Preparation of PEG-Peptide-PTX-Solid Lipid Nanoparticles (Pp-PTX-SLNs)

Preparation of PTX-SLNs

PTX-SLNs, the hydrophobic core of Pp-PTX-SLNs, were prepared by adapting the film ultrasonication method described by Nikanjam *et al.* (17). SPC, medium-chain triglycerides (MCT), GMS and OA were formulated together in the molar ratio of 3:1:1:0.6 in order to optimize particle stability and zeta potential. The lipid mixture and PTX were dissolved in methanol and dried in a rotary evaporator (Rotavapor R-3, BUCHI, Switzerland) under reduced pressure at 45°C to remove the solvent. The dried lipid film was re-dispersed in 0.1% F68 aqueous solution (pH 7.4) with shaking for 1 min. The resultant suspension was sonicated (IY92-2 Ultrasonic cell crusher, Shanghai, China) at 200 W and 4°C for 1.5 min, and extruded first through 0.8-μm and then through 0.45-μm filters to obtain the desired colloidal PTX-SLNs dispersion.

Conjugation of PEG-Peptides to the Surface of PTX-SLNs

EDC·HCl (14.5 mg) and NHS (8.5 mg) were added to aqueous PEG-peptide solution (1 mL), and the mixture was gently stirred for 15 min at room temperature. Then the aqueous solution was mixed with PTX-SLN suspension in the weight ratio of 1:2 (PEG-peptides/lipid) to yield Pp-PTX-SLNs. The resulting suspension was incubated at 37°C for 2 h with gentle agitation, and then centrifuged in an ultrafiltration tube (Millipore, 4 mL, MW cut-off 10 kDa) at 4,000 g for 20 min to remove the unbound PEG-peptide and free PTX. Finally, the Pp-PTX-SLN dispersion was lyophilized (Savant Modulyo, Savant, USA). Control nanoparticles were prepared following the same methods described above to examine the specificity of MMP substrate cleavage (Pp'-PTX-SLNs) and the influence of Pp (PTX-SLNs).

Determination of Conjugation Efficiency of the PEGylated Peptide

The efficiency of PEGylated peptide conjugation to the surface of SLNs was determined using the bitter acid spectrophotometric method (18) by spectrophotometric determination of complexes of polyethers and sodium ions, which form ion pairs with picrate anion when extracted into 1,2-dichloroethane. Because high lipid concentrations can interfere with the determination of conjugation efficiency, samples were diluted to a lipid concentration of ≤0.2 mM (18).

Conjugation efficiency (CE) was determined by mixing the sample solution (5 mL) with 10 mL of pre-prepared sodium nitrate-picrate solution (0.1 M sodium hydroxide, 3.3 M sodium nitrate and 0.02 M picric acid), followed by addition of 5 mL of 1,2-dichloroethane. The solution was mixed thoroughly and centrifuged at 3,600 g for 10 min; the organic layer was collected into a new tube, and the spectrophotometric absorbance at 378 nm was determined. Using a previously constructed calibration curve of standard PEGylated peptide solution, the CE% of PEGylated peptide was determined:

$$\mathrm{CE}(\%) = (\text{PEG-peptide on SLN surface}/\text{Total PEG-peptide}) \times 100\%$$

Characterization of Pp-PTX-SLNs, Pp'-PTX-SLNs and PTX-SLNs

Morphology, Particle Size and Zeta Potential of the Nanoparticles

The morphology of the SLNs was studied by transmission electron microscopy (TEM, H-600, Hitachi High-Technologies Corporation). To be specific, samples for TEM were loaded on the copper grid followed by negative staining with uranyl acetate (1% w/v) for 10 min. Next, the spare dye was gently blotted with filter paper and samples were air-dried to completely remove the water. Then, the

samples were observed under the TEM. The diameter, zeta potential and the polydispersity index of the SLNs were determined by the Malvern Zetasizer Nano ZS90 instrument (Malvern instruments Ltd., U.K.). Measurements were performed at 25°C and equilibrium time was 1 min with automatic cycles of measurement determined by the instrument.

Determination of Encapsulation Efficiency and Drug Loading

Encapsulation efficiency and drug loading were assessed by subjecting the samples to size exclusion chromatography. Nanoparticle samples were loaded on a pre-equilibrated Sephadex G-50 column (10 mm × 200 mm) and eluted with ultrapure water to separate free PTX from nanoparticles. Fractions eluting at different times were demulsified in methanol (1:2, v/v) to obtain monophase solutions.

The amount of PTX in 20 μL of each fraction was determined by HPLC (Agilent 1260, Agilent, USA). A reverse-phase C18 column (4.6 mm × 150 mm, 5 μm, Dikma) was flushed with mobile phase containing acetonitrile and ultrapure water (55:45, v/v) at a flow rate of 1.0 mL/min. The detection wavelength was 227 nm, and column temperature was maintained at 35°C. A calibration curve was constructed using PTX solution concentrations ranging from 0.05 to 500 μg/mL. The encapsulation efficiency (EE%) and drug loading (DL%) were calculated using the following equations respectively (19):

$$EE\% = (\text{PTX in nanoparticles}/\text{Total PTX in dispersion}) \times 100\%$$
$$DL\% = (\text{PTX in nanoparticles}/\text{Total lipid in dispersion}) \times 100\%$$

In Vitro Drug Release

In vitro release of PTX from Taxol®, PTX-SLNs and Pp-PTX-SLNs were investigated at 37°C in PBS buffer (pH 7.4) containing 0.1% Tween-80. PTX-loaded formulations (approximately 4 mg of total lipids) were suspended in 1 mL PBS and dialyzed against 50 mL PBS buffer at 37°C using a dialysis membrane (MW cut-off 8 kDa) with shaking at 100 rpm. Samples (1.0 mL) of dialyzed solution were aspirated at various times, and the same volume of fresh buffer was added to maintain the volume. All samples were centrifuged at 16,000 g for 10 min, and PTX levels in the supernatants were determined using HPLC as described above. Care was taken to protect the samples from light throughout the experiment.

Cytotoxicity Evaluation *In Vitro*

The cytotoxicity of various concentrations of SLNs was evaluated by MTT assay. HT1080 cells were seeded in 96-well plates at a density of 1×10^4 cells/well and incubated for 24 h. Then, the medium was replaced by different amounts of Pp-PTX-SLNs, PTX-SLNs or SLNs in DMEM-HG medium (without FBS, pH 7.4). After 4 h of incubation, the medium containing each formulation was replaced with complete medium followed by incubation for another 24 h. Then 10 μL of MTT solution (5 mg/mL in PBS, pH 7.4) was added and the plates were incubated for another 4 h at 37°C in the dark. Afterwards, the medium was removed and 150 μL of DMSO was added in order to solubilize the formazan crystals, and the plates were incubated for 10 min at 37°C with gentle shaking. The absorbance of each well was measured at 570 nm using a microplate reader (Thermo Electron Corporation). Cell viability was calculated using the following equation:

$$\text{Cell viability}(\%) = OD_s/OD_{control} \times 100\%$$

where OD_s is the absorbance intensity of the cells treated with different formulations, while $OD_{control}$ is the average absorbance intensity of the cells incubated only with culture medium.

Cellular Uptake

Analysis by fluorescence Microscopy

MMPs are highly expressed in HT1080 and LLC cells and poorly expressed in CHO cells (20), hence these cells were used. These three types of cells were seeded at a density of 1×10^6 cells/well on pretreated cover slips. After 24 h, the medium was replaced with 50 μg/mL of Pp-SLNs, Pp'-SLNs or SLNs (all loaded with coumarin-6) diluted in DMEM-HG (without FBS, pH 7.4). Cells were incubated with the nanoparticle mixtures for 4 h, then the supernatant was removed, cells were washed three times with PBS, and cover slips were observed by fluorescence microscopy (ZEISS-HBO 50).

Analysis by Flow Cytometry

HT1080, LLC and CHO cells were seeded in 6-well plates at a density of 1×10^6 cells/well and incubated in complete medium for 24 h. The medium was removed and cells were treated with different SLN formulations as described above. After incubation, supernatants were removed and cells were washed three times with ice-cold PBS. All samples were re-suspended in PBS and analyzed by flow cytometry (Beckman Coulter).

In Vivo Tumor Targeting

Pharmacokinetic Studies

C57BL/6 N male mice (6 to 8 weeks old) were purchased from the Laboratory Animal Center of Sichuan University. All animal tests were approved by the Animal Ethics committee of Sichuan University West China Medical School, and all procedures with animals were conducted according to the guidelines of the local Animal Use and Care Committees of Chengdu and executed

according to the National Animal Welfare Law of China. C57BL/6 N mice were subcutaneously implanted with LLC cells in the right back flank at a density of 1×10^6 cells per mice. The tumor was allowed to grow for approximately 15 days until it reached 10-15 mm^3 in size.

To investigate the systemic circulation time of each type of nanoparticle, they were loaded with the hydrophobic1,1′-dioctadecyl-3,3,3′,3′-tetramethylindodicarbocyanine and 4-chlorobenzenesulfonatesalt (DiD) fluorophore (exCitation/emission, 644/655 nm). This dye is commonly used as a marker in circulation studies of nanoparticles and has minimal leakage *in vivo* (<20% over 72 h) (21).

Formulations of Pp-DiD-SLNs, Pp'-DiD-SLNs and DiD-SLNs (100 μL, 5 mg/mL, containing 1.5 μg DiD) were injected into mice through the tail vein and each formulation was tested in six mice. Blood (20 μL)was collected from the retro-orbital vein at 1, 5, 15, and 30 min and at 1, 2, 4, 8, 24, and 48 h after administration. Blood samples were diluted with 30 μL of PBS in a 96-well plate and subjected to fluorescence measurements using a VarioskanFlash instrument (Thermo Scientific). Pharmacokinetic parameters were calculated using a two-compartment model and a one-way nonlinear model.

In Vivo Distribution of PTX

The tumor mouse model described in the above section was used to determine whether PEG-peptide prolongs circulation time of the nanoparticles and whether it interacts with tumor-overexpressed MMPs to facilitate the entry of nanoparticle into tumor cells. Pp-PTX-SLNs, Pp'-PTX-SLNs, PTX-SLNs or Taxol® were administered to animals ($n=5$) intravenously through the tail vein at a dose of 10 mg/kg. At 0.25, 1, 6, 12, and 24 h after administration, mice were sacrificed and samples of blood, tumor and other tissues were collected. Non-blood tissue samples were rinsed with PBS, homogenized, suspended in methyl alcohol to precipitate protein, and then centrifuged. The concentration of PTX in the supernatant was detected by HPLC.

In Vivo Anti-Tumor Activity

Mice bearing LLC tumors were obtained as described above and housed under standard conditions for 10 days, after tumor size had reached approximately 8-12 mm^3. Mice ($n=10$) were injected intravenously with Pp-PTX-SLNs, Pp'-PTX-SLNs, PTX-SLNs or Taxol® at a dose of 10 mg/kg, and tumor growth and survival time were measured. Tumor volume was measured using the following formula:

$$\text{Tumor volume} = 1/2\left(\text{length} \times \text{width}^2\right)$$

Statistical Analysis

All experiments in this study were repeated at least three times, and data were presented as mean ± standard deviation. Unpaired Student's t test was used for comparison between-groups. Data were considered to be statistically significant if $P<0.05$(*) and highly significant if $P<0.01$ (**).

RESULTS

Assay of MMP Concentration and Activity

Secretion of MMPs from HT1080 and LLC cells was evaluated by gelatin zymography. Zymographic imaging showed that the two tumor cell lines secreted different concentrations and types of MMPs (Fig. 1). The molecular weight of the MMPs detected were consistent with those of MMP-2 (72 kDa) and MMP-9 (92 kDa) (22). Both cell lines secreted higher level of MMP-2 than MMP-9, and HT1080 cells secreted a higher overall level of MMPs than did LLC cells.

Preparation of Pp-PTX-SLNs

Preparation of Pp-PTX-SLNs and Measurement of Conjugation Efficiency

Solid lipid cores of PTX-SLNs were prepared with SPC, MCT, GMS, OA and PTX using the film ultrasonication method. A modicum of OA (OA:lipids =1:9) was incorporated to increase the positive charge of SLNs. The amino groups exposed on the nanoparticle surface serve as conjugation sites with PEGylated peptide. The encapsulation efficiency and drug loading of PTX-SLNs were 75% and 7% respectively.

The conjugation efficiency of PEGylated peptide linkage to SLNs was determined using the bitter acid spectrophotometric method (18). Higher mass ratios of PEGylated peptide:OA gave slightly higher conjugation efficiencies (data not shown). A mass ratio of 10:1 gave the optimal conjugation efficiency (26.5 ± 0.06%).

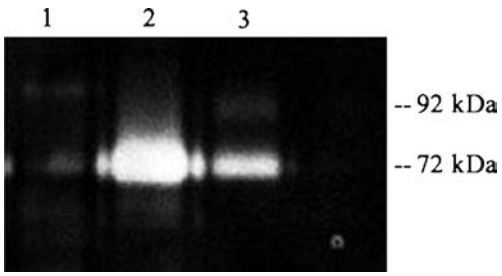

Fig. 1 Zymography of control MMPs (*lane 1*), conditioned medium of HT1080 cells (*lane 2*), and conditioned medium of LLC cells (*lane 3*). The approximate molecular weights of MMP-2 (72 kDa) and MMP-9 (92 kDa) are shown.

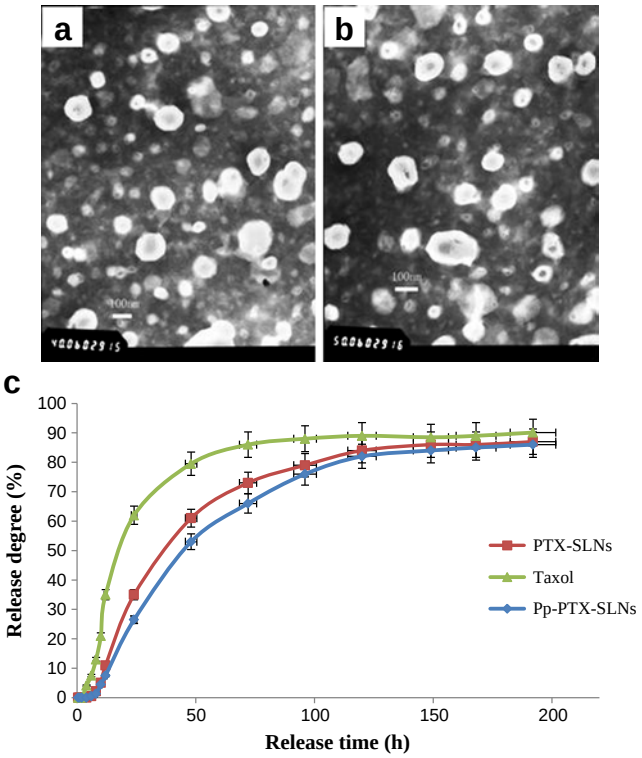

Fig. 2 TEM images of (**a**) non-modified PTX-SLNs and (**b**) Pp-PTX-SLNs. Bar: 100 nm. (**c**) Cumulative release of PTX *in vitro* from Taxol®, PTX-SLN and Pp-PTX-SLNs in PBS (pH 7.4) with 0.1% Tween-80 at 37°C. Results are presented as mean ± SD ($n = 3$).

Morphology, Particle Size and Zeta Potential

TEM images of Pp-PTX-SLNs (Fig. 2a) and PTX-SLNs (Fig. 2b) showed spherical and homogeneous vesicles. The average diameter of Pp-PTX-SLNs (120 ± 3.5 nm) was larger than that of unmodified PTX-SLNs (100 ± 2.2 nm), and nanoparticles of both formulations had narrow size distribution (polydispersion index <0.03). Zeta-potential measurements showed that Pp-PTX-SLNs had positive charge of 30.5 ± 1.2 mV and PTX-SLNs had a charge of 41.1 ± 1.9 mV. These results show that conjugating the PTX-SLNs with PEGylated peptide slightly increased nanoparticle size and slightly decreased the intensity of the positive surface charge.

In Vitro Release

Figure 2c shows the cumulative profiles of PTX release from Pp-PTX-SLNs and PTX-SLNs, as well as the release of Taxol®. Most PTX in Taxol® was released in an early burst, whereas the PEGylated and unmodified SLNs showed biphasic release of PTX. An initial, minor burst was followed by significant and stable release over a prolonged period. After 50 h, nearly 80% of Taxol® was released, compared to only 60% of PTX from PTX-SLNs and 50% from Pp-PTX-SLNs. The rate of PTX release was slower from Pp-PTX-SLNs than from PTX-SLNs.

In Vitro Cytotoxicity

The cytotoxicity of blank nanoparticles and the three types of PTX-loaded nanoparticles on HT1080 cells was measured using the MTT assay. As a control, the toxicity of Taxol® was tested in parallel. Blank SLNs modified or not with PEGylated peptide did not induce apparent toxicity in HT1080 cells even at the highest concentration investigated (400 μg/mL), since the cell viability was >90%. Adding OA to SLNs did not significantly affect the viability of HT1080 cells (Fig. 3a), whereas OA concentrations >250 μg/mL slightly inhibited cell growth. Different formulations of empty SLNs were not associated with significantly different levels of cytotoxicity.

PTX-loaded nanoparticles caused obvious toxicity in cells. The IC_{50} of Taxol®, PTX-SLNs, Pp-PTX-SLNs and Pp'-PTX-SLNs was 2.77 ± 0.19, 0.34 ± 0.02, 0.40 ± 0.03 and 0.83 ± 0.05 μg/mL for HT1080 cells, respectively. Overall, the relative toxicity was PTX-SLNs > Pp-PTX-SLNs > Pp'-PTX-SLNs > Taxol® (Fig. 3b). The significant differences in cell cytotoxicity among the three types of SLNs and Taxol® could be attributed to their different nanoparticle sizes and the presence or absence of cleavable PEG-peptides.

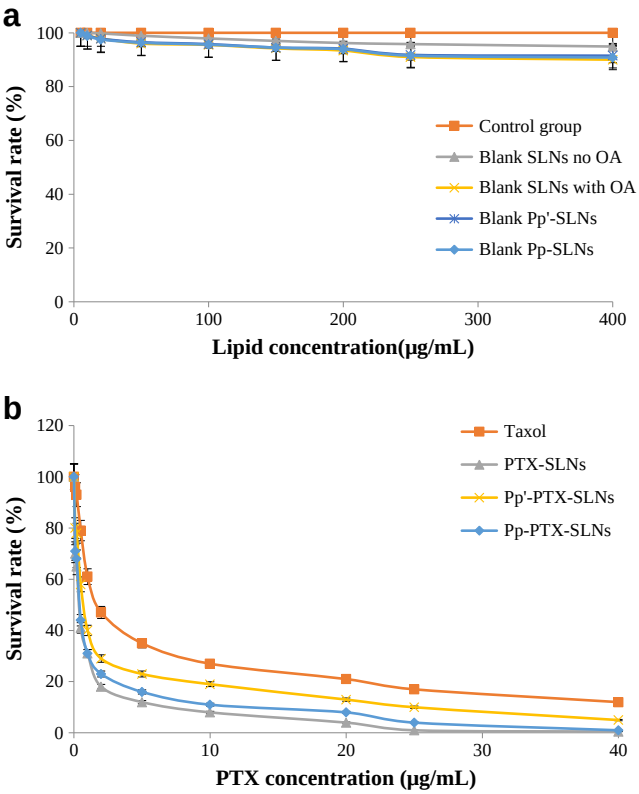

Fig. 3 (**a**) *In vitro* cytotoxicity of empty SLNs in HT1080 cells at 37°C after incubation at concentrations ranging from 5 μg/mL to 400 μg/mL. (**b**) Cytotoxicity of PTX-SLNs, Pp'-PTX-SLNs and Pp-PTX-SLNs in HT1080 cells at 37°C after incubation at concentrations from 0.1 μg/mL to 40 μg/mL. Results are presented as mean ± SD ($n = 3$).

Cellular Uptake

Internalization of coumarin-6-loaded Pp-SLNs, Pp'-SLNs and SLNs into HT1080, LLC and CHO cells was studied by using fluorescence microscopy. In HT1080 and LLC cell lines, cellular uptake of Pp-SLNs was lower than that of unmodified SLNs (Fig. 4a), consistent with the ability of the PEG chain to impede vehicle uptake. Fluorescence intensity was much higher for Pp-SLNs than for Pp'-SLNs. However, there was no significant difference in fluorescence intensity between Pp-SLNs and Pp'-SLNs in CHO cells, which express lower levels of MMPs than the other two cell lines. These results suggest that the PEG chain was removed from the SLNs in response to specific cleavage by MMPs. Flow cytometry confirmed and extended these findings. At a concentration of 50 μg/mL, PTX-SLNs showed the highest cellular uptake efficiency, approximately 1.47-fold higher than that of Pp-PTX-SLNs and 2.11-fold higher than that of Pp'-PTX-SLNs (Fig. 4b). Significantly more Pp-PTX-SLNs were taken up than Pp'-PTX-SLNs ($P<0.01$). These results suggest that the PEG-peptide was cleaved by tumor-overexpressed MMPs, enhancing drug internalization.

In Vivo Experiments

Pharmacokinetic Studies

First, the pharmacokinetic behavior of PTX incorporated in different SLN formulations was modeled by measuring the persistence of the fluorophore DiD in plasma after intravenous administration of Pp-DiD-SLNs, Pp'-DiD-SLNs and DiD-SLNs into mice. Fluorescence curves of DiD in mouse plasma over time after administration of nanoparticles at a dose of 22.5 mg/kg are shown in Fig. 5. As expected, unmodified SLNs were cleared most rapidly *in vivo* by 4 h post-injection, and the fluorescence signal of DiD in SLNs was below the limit of detection. In contrast, the relative fluorescence signal of the PEG-modified SLNs was over 50% at 10 h post-injection. The fluorescence curves for Pp-SLNs and Pp'-SLNs did not show significant differences.

In addition, the pharmacokinetic parameters of PTX in plasma after intravenous injection were measured. As observed with DiD-loaded nanoparticles, PEG modification of PTX vehicle significantly prolonged elimination half-life ($t_{1/2}$), decreased clearance rate (CL) and increased $AUC_{0\text{-}24h}$ compared with Taxol® and PTX-SLNs (Table II) ($p<0.01$).

In Vivo Distribution

The biodistribution of Taxol®, Pp-PTX-SLNs and PTX-SLNs in tumor-bearing mice was evaluated. Taxol® distributed rapidly into various tissues within 0.25 h after intravenous administration (Fig. 6), with the greatest accumulation being in liver (56%). By 1 h after administration, Taxol® concentration increased in heart and lung, while only small amounts were visible in the tumor and plasma. The three types of nanoparticles displayed distribution patterns that differed from that of Taxol® and from one another. By 0.25 h after intravenous injection, the nanoparticles were present primarily in plasma, while Pp-PTX-SLNs and Pp'-PTX-SLNs showed some accumulation at tumor sites. After 1 h, the amount of PTX-SLNs in the plasma decreased considerably, while the amount of Pp-PTX-SLNs and Pp'-PTX-SLNs decreased only slightly. At 12 h after administration, the accumulation in tumors was according to the following order: Pp-PTX-SLNs > Pp'-PTX-SLNs > PTX-SLNs > Taxol®. Analysis of relative $AUC_{0\text{-}24h}$ values for Pp-PTX-SLNs, Pp'-PTX-SLNs, PTX-SLNs, and Taxol® in different tissues (Table I) showed that accumulation in tumor was 4.25-fold higher for Pp-PTX-SLNs than for Taxol®, whereas it was only 1.17-fold higher for PTX-SLNs than for Taxol®. Furthermore, the amount of Pp-PTX-SLNs at tumor sites was significantly (1.62-fold) higher than that of Pp'-PTX-SLNs ($p<0.05$). These results suggest that Pp-PTX-SLNs circulated longer in the blood than did PTX-SLNs and Taxol® and were able to reach tumor tissues *in vivo* as a result of the EPR effect and tumor-specific surface peptide cleavage.

Anti-Tumor Efficacy

To assess the therapeutic potential of Pp-PTX-SLNs, the effects of Taxol®, PTX-SLNs, Pp'-PTX-SLNs and Pp-PTX-SLNs on tumor volume and survival time in LLC tumor-bearing mice were evaluated. Mice were dosed intravenously with the PTX-loaded formulations, and control mice were treated with saline buffer. All formulations containing PTX inhibited the tumor growth in the following order: Pp-PTX-SLNs > Pp'-PTX-SLNs > Taxol® = PTX-SLNs. Survival time was significantly longer in the mouse group administered Pp-PTX-SLNs (39 days) than in the other animal groups (log-rank analysis relative to Pp-PTX-SLNs: Pp'-PTX-SLNs, $p<0.05$; PTX-SLNs, $p<0.01$; Taxol®, $p<0.01$; saline, $p<0.01$). These results suggest that conjugating PTX-SLNs with tumor-specific PEG-peptide can enhance the effect of PTX administered systemically.

DISCUSSION

In this study, we have developed an SLN drug delivery system for anticancer treatment and explored its safety and efficacy using *in vitro* and *in vivo* investigations. *In vitro* experiments on two tumor cell lines showed that the SLNs coated with enzymatically cleavable PEG(Pp-PTX-SLNs) were taken up by cells to a greater degree than SLNs bearing the conventional PEG-lipid (Pp'-PTX-SLNs). *In vivo* experiments using tumor-

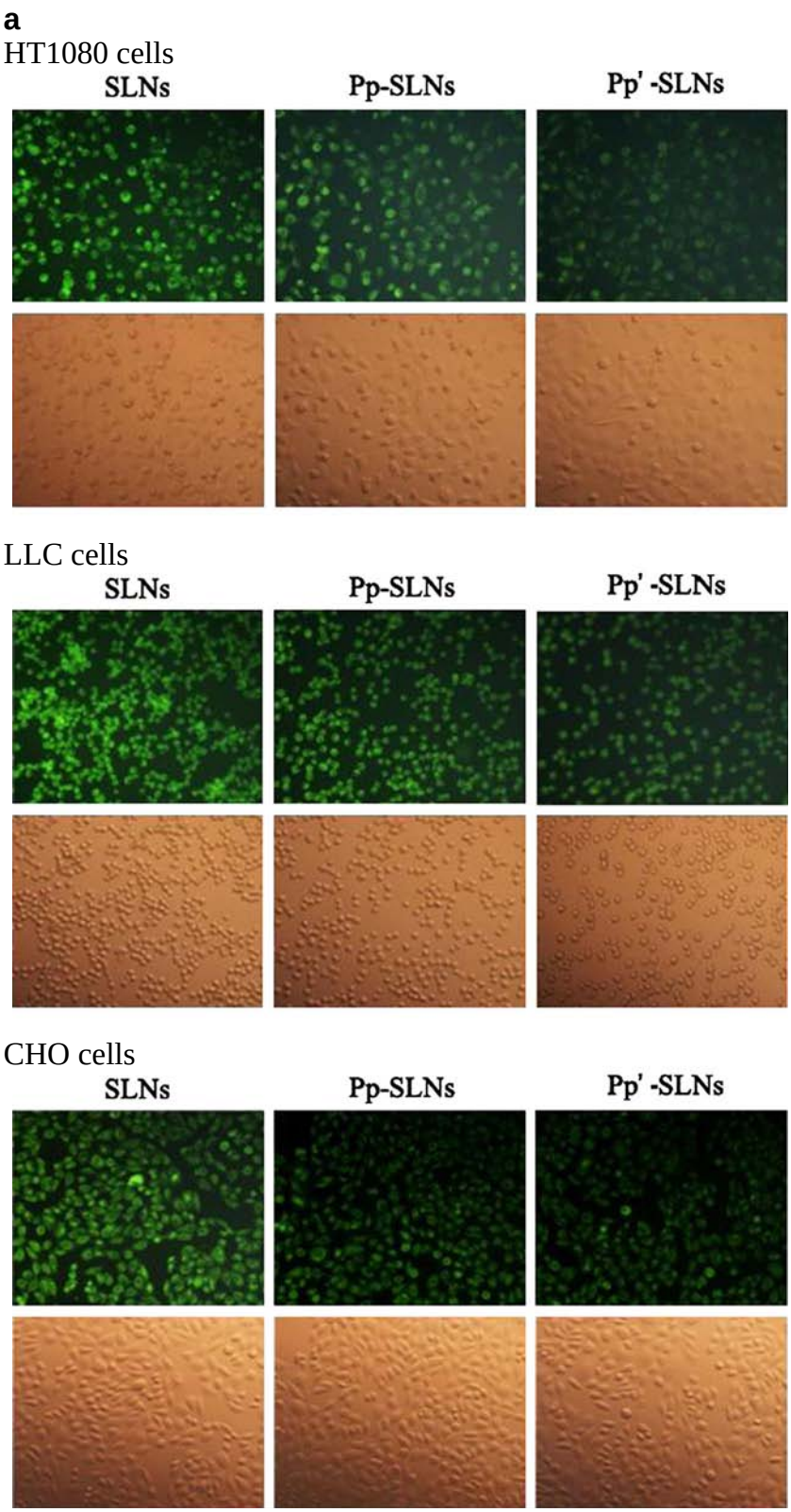

Fig. 4 (**a**) Fluorescence microscopy images of cellular uptake of coumarin-6-labeled unmodified SLNs, Pp'-SLNs and Pp-SLNs by HT1080, LLC and CHO cells at 37°C after 4-h incubation with the indicated nanoparticles at a concentration of 50 μg/mL. (**b**) Quantitation of cellular uptake of coumarin-6-labeled unmodified SLNs, Pp'-SLNs and Pp-SLNs by HT1080, LLC and CHO cells at 37°C after 4-h incubation with the indicated nanoparticles at a concentration of 50 μg/mL ($n = 3$). Fluorescence intensity is proportional to the extent of cell uptake and the fluorescence intensity of blank cells was measured as a control. Statistical significance of comparisons is as follows: Pp-SLNs and Pp'-SLNs *vs* SLNs, $^{*}p < 0.05$; Pp-SLNs *vs* Pp'-SLNs, $^{\#}p < 0.01$. Results shown are mean ± SD values ($n = 3$).

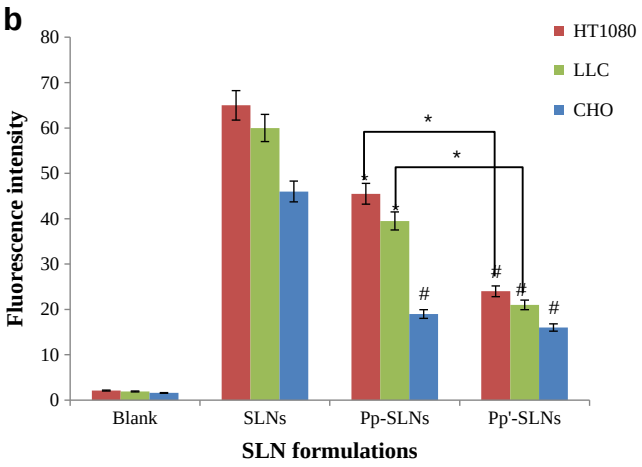

Fig. 4 (continued)

bearing mice showed that Pp-PTX-SLNs delivered higher drug concentrations to tumor tissues and had better anti-tumor efficacy than did Pp'-PTX-SLNs. These results suggest that SLNs coated with PEGylated MMP substrate peptide may represent excellent potential as vehicles for delivering drugs rapidly and specifically to tumor sites.

Our drug delivery system exploits the advantages of long-chain PEG molecules for preventing nanoparticle phagocytosis, while minimizing their disadvantages for nanoparticle uptake and drug activity. PEGylation technology has been widely used to enhance the pharmacokinetics of a variety of nanoparticles, because the hydrophilic, inert PEG creates a steric barrier on the surface of nanoparticles and minimizes protein binding with plasma, interfering with the primary mechanism by which RES recognizes circulating nanoparticles (23). At the same time, PEGylation inhibits cellular uptake and affects the intracellular trafficking of nanoparticles, especially their ability to escape from endosomes, markedly reducing drug activity (11). In addition, the prolonged circulation time increases the exposure of other tissues to the drug, which increases the risk of adverse effects. For instance, the stealth liposomes of doxorubicin introduced unexpected side effects such as hand-foot syndrome and mucositis in the clinic (24).

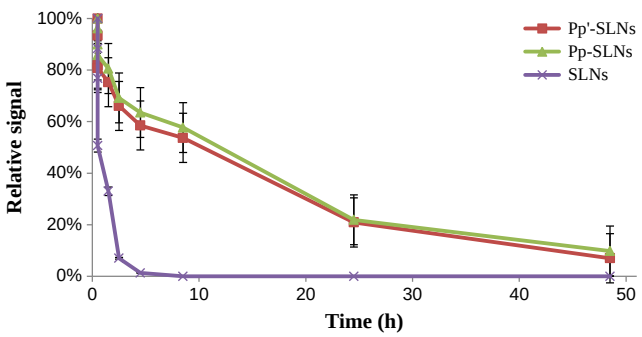

Fig. 5 Relative DiD fluorescence-time curves in plasma for SLNs, Pp'-SLNs and Pp-SLNs after intravenous administration at a nanoparticle dose of 22.5 mg/kg ($n = 6$). Results shown are means ± SD values ($n = 3$).

Thus, de-PEGylation technology such as the approach used in our delivery system is needed to produce a safer, and more potent drug formulation, offering the advantage of RES evasion and avoiding the adverse effects due to excessive prolonged circulation time.

Our de-PEGylation strategy relies on a PEGylated MMP-2 substrate peptide (13,15) containing the PLGI cleavage site, which can also be cleaved by MMP-3, MMP-7, MMP-8, and MMP-9 (13). This approach presents advantages over others reported in the literature. For example, one strategy is by linking PEG molecules to 1,2-Distearoyl-sn-Glycero-3-Phosphoethanolamine (DSPE) through a cleavable disulfide bridge (PEG-S-S-DOPE) (25). Unfortunately the disulfide bridge proved unstable *in vivo*, and addition of exogenous reducing agent was almost always required in order to cleave the disulfide bond (26). In another approach, it was attempted to design a pH-sensitive link by joining the PEG and lipid with an acid-labile single vinyl ether linkage. The problem with this strategy is that the most acidic sites in tumors often lie distal from the tumor microvasculature, where the nanocarriers cannot penetrate (27). The success of our approach exploiting MMP cleavage is consistent with the fact that these enzymes, which are secreted by tumor microvascular endothelial cells (28), are known to be important for degrading the extracellular matrix around the growing tumor (29).

The success of our system was essentially attributed to using the aliphatic amine OA to conjugate the MMP-specific cleavable PEG-peptide to the SLN surface. Using this linkage, the amino group of OA binds to the carboxyl group of the peptide. The hydrophilic amino group is exposed on the surface, while the hydrophobic hydrocarbon moiety is incorporated into SLNs. When the molar ratio of PEGylated peptide to OA is 1:1, there should theoretically be no free amino groups. However, under our conditions, we detected a small fraction of free amino groups internalized in SLNs by the ninhydrin coloration method. Presumably this reflected the fact that lipid-soluble OA was encapsulated in the nanoparticles and some amino groups were inaccessible to the PEGylated peptide. This may explain why we did not succeed to increase the conjugation efficiency even after increasing the mass ratio of PEGylated peptide to OA to 12:1.

We determined the optimal conjugation efficiency of PEG-peptide on the surface of nanoparticles to be 26.5±0.06%, corresponding to a molar ratio (with respect to lipids) of 2.65% of conjugated PEG_{2000}-peptide on the SLN surface. This is consistent with a previous study reporting that a molar ratio of 2% PEG_{2000} on the nanoparticle surface was adequate for the polymer molecules to cover the entire particle surfaces (30). This suggests that the surfaces of our SLNs were completely coated with the cleavable PEGylated peptide.

Nanoparticle size is one of the most important parameters for determining the *in vitro* and *in vivo* behavior of nano-based drug delivery systems (31). Previous work suggested that

Table I AUC (%) of PTX-SLNs, Pp'-PTX-SLNs and Pp-PTX-SLNs (Relative to Taxol®) in Different Tissues of C57 Mice After 24 h Treatment with 10 mg/kg PTX ($n=5$)

AUC_{0-24} (%)	Taxol®	PTX-SLNs	Pp'-PTX-SLNs	Pp-PTX-SLNs
Heart	1.00	1.35*	0.23#	0.19#
Liver	1.00	0.956	0.782*	0.729*
Spleen	1.00	0.767	1.18	1.05
Lung	1.00	0.878	0.469*	0.176#
Kidney	1.00	0.884	1.005	1.043
Plasma	1.00	1.45*	12.5#	11.3#
Tumor	1.00	1.17	3.30*	5.35#

Significantly different from the Taxol® group:*$p<0.05$, #$p<0.01$

nanoparticles of 100-150 nm accumulated better in tumors as a result of the EPR effect (32). Our Pp-PTX-SLNs had a size in this range, as well as the expected hydrophilic surface (Fig. 2a). These physicochemical characteristics may explain why the Pp-PTX-SLNs showed a biphasic PTX release profile (Fig. 2b). The initial burst release was likely to be due to drug concentrated at or near the particle surface that quickly entered the surrounding medium. The subsequent sustained release was due to slow diffusion of the drug from the interior of the particles to the exterior environment. As a result of this second phase, drug was steadily released over 120 h. Taxol®, in contrast, showed only a single burst release phase, suggesting that nanoparticle encapsulation and PEG modification can alter the release pattern of anticancer drugs like Taxol® and the nanoparticle-based drug delivery systems such as ours may reduce the need for frequent drug administration, offering clear advantages over Taxol® the clinically established and widely used formulation of PTX.

The cytotoxicity of empty and drug-loaded SLNs on HT1080 cells was evaluated by measuring cell viability in the MTT assay. Empty SLNs lacked observable cytotoxicity (Fig. 3a), even at the highest concentration investigated (400 μg/mL). This suggests that the lipids themselves have low cytotoxicity. In contrast, the cremophor:ethanol (1:1, v/v) in the commercial vehicle of PTX (Taxol®) has been reported to be highly toxic to normal human foreskin fibroblast cells in the MTT assay (33). Therefore, encapsulating PTX with SLNs may be less toxic than other conventional delivery systems. We found PTX-SLNs to cause the highest cytotoxicity, followed by Pp-PTX-SLNs, and then Taxol®. One research group reported that PTX-SLNs are likely to be internalized via endocytosis, specifically clathrin-mediated endocytosisb (34). The observation that PTX-SLNs are more toxic than free PTX may be attributed to the greater uptake and intracellular accumulation of the nanoparticles.

Table II Pharmacokinetic Parameters of PTX Delivered at a Dose of 10 mg/kg Intravenously to C57 mice ($n=5$) in The Form of Taxol®, PTX-SLNs, Pp'-PTX-SLNs orPp-PTX-SLNs

Parameter	Taxol®	PTX-SLNs	Pp'-PTX-SLNs	Pp-PTX-SLNs
$AUC_{(0-24)}$ (μg/L/h)	2190	3176*	27375#	24747#
k (h^{-1})	0.45	0.39	0.15#	0.13#
$t_{1/2}$ (h)	1.94	2.16*	12.92#	14.761#
CL (L/h)	1.61	0.915	0.10#	0.12#

Abbreviations: AUC_{0-24} area under curve, *K* elimination rate constant, $t_{1/2}$ elimination half-life, *CL* total clearance rate

Significantly different from the Taxol® group:*$p<0.05$, #$p<0.01$

Our cell uptake studies revealed the importance of sequence-specific peptide cleavage for our drug delivery system. Uptake of Pp-SLNs was significantly higher than that of Pp'-SLNs (Fig. 4) ($p<0.01$). These *in vitro* uptake results were also confirmed *in vivo*. Pp-PTX-SLNs accumulated significantly more in the tumor tissue than did Pp'-PTX-SLNs ($p<0.05$), illustrating the importance of tumor-specific cleavage of the PEG-peptide for efficient drug delivery.

Our pharmacokinetic studies *in vivo* indicated that after intravenous injection through the tail vein, non-PEGylated SLNs were quickly removed from the circulation (Fig. 5). In contrast, Pp-SLNs and Pp'-SLNs showed slower blood clearance. The accumulation of Pp-SLNs in the plasma (20%) and elimination half-life (14.76 h) that we observed in the present study were higher than the corresponding values in literature for PEG-PTX-SLNs (10%, 7.21 h) or transferrin-coupled PEG-PTX-SLNs (10%, 6.56 h) (35). The half-life time in our study (14.76 h) was also longer than the half-life values reported by Chen and co-workers (2001) for PTX-SLNs (10.06 h) containing stearic acid, lecithin, poloxamer F68 and PEG-DSPE (36). These differences may reflect differences in PEG chain length or molar ratio of PEG to lipids. In all cases, the results suggest that conjugating PEG-peptide to the SLN surface significantly prolongs circulation time *in vivo* ($p<0.01$), likely by preventing rapid uptake by the mononuclear phagocyte system, giving Pp-PTX-SLNs better chances to reach the tumor site.

The longer circulation time of Pp-PTX-SLNs, Pp'-PTX-SLNs, and PTX-SLNs was possibly responsible for the distribution to be mainly in the plasma, whereas Taxol® was distributed mainly in liver, kidney, lung, and heart, (Fig. 6, Table I). These results with Taxol® are consistent with previous work (37). Whereas the level of PTX-SLNs in plasma decreased rapidly, that of Pp-PTX-SLNs and Pp'-PTX-SLNs decreased much more gradually. Beyond 6 h post-injection, Taxol® was gradually eliminated from all tissues, whereas Pp-PTX-SLNs and Pp'-PTX-SLNs were transported from the plasma into normal tissues to different extents, similar to results reported for PEG-SLNs (35). Pp-PTX-SLNs were unique with respect to their ability to accumulate in tumor tissue until reaching 16.5%, approximately 2.5-fold higher than the distribution of 6.7% observed with PEG-SLNs in another study (35).

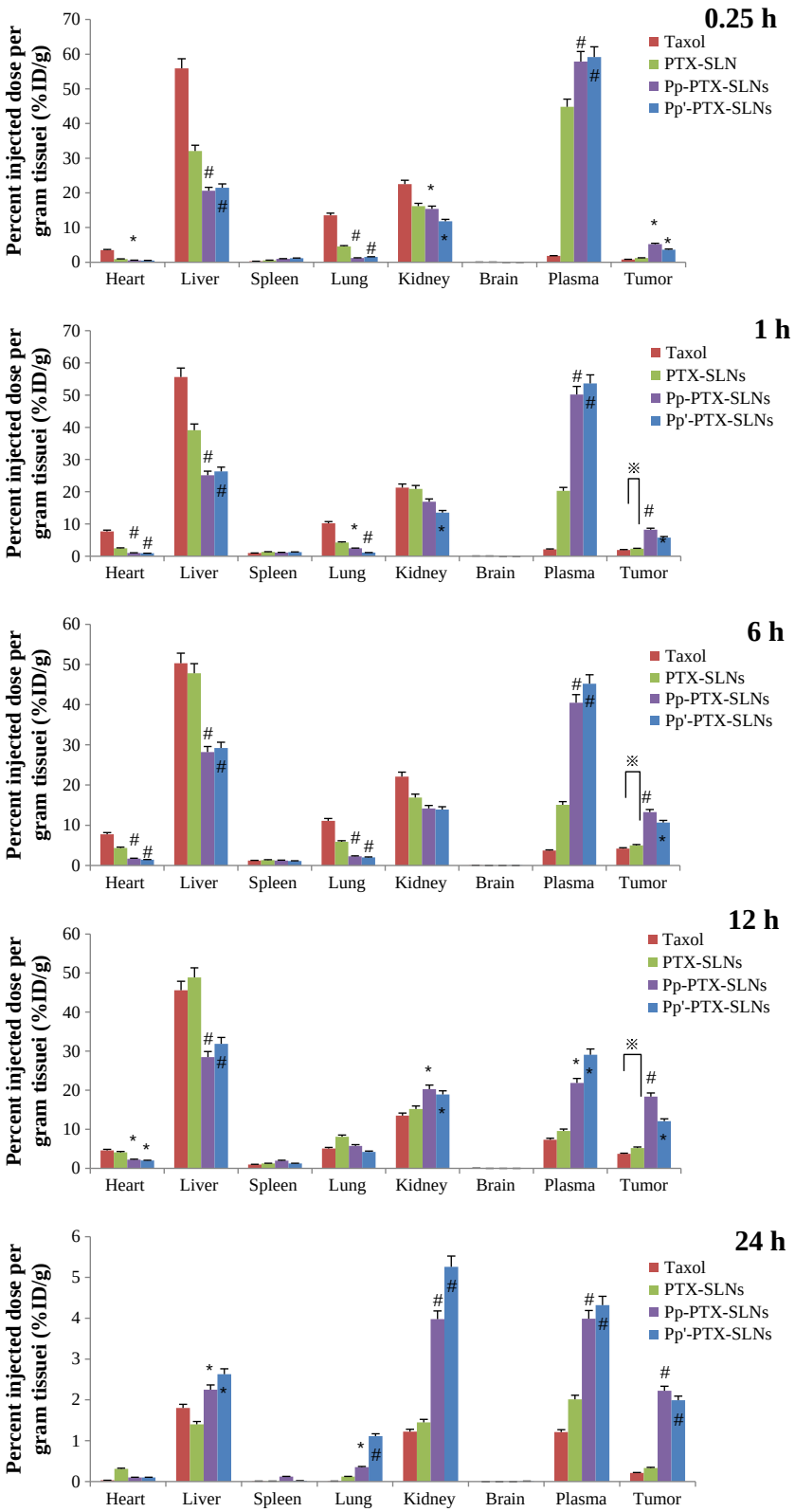

Fig. 6 Tissue distribution of Taxol®, PTX-SLNs, Pp'-PTX-SLNs and Pp-PTX-SLNs in C57 mice bearing LLC tumors at 0.25, 1, 6, 12, and 24 h after intravenous injection ($n = 5$ for each group and each time point).*$p < 0.05$, #$p < 0.01$ compared with Taxol®-treated group; Pp'-PTX-SLNs *vs* Pp-PTX-SLNs, ※$p < 0.05$. Results are presented as mean ± SD.

Our Pp-PTX-SLNs showed excellent tumor targeting compared not only to Taxol® but also to other PEGylated nanoparticles. PEGylated PTX-nanoparticles PLA-TPGS NPs showed an AUC of 1.6 relative to Taxol® (38), whereas our Pp-PTX-SLNs showed a relative AUC of 5.35. The accumulation rate of albumin PTX nanoparticles

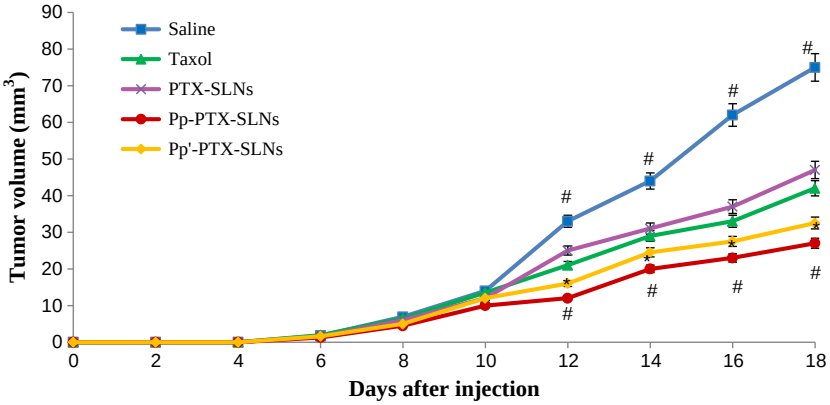

Fig. 7 Tumor volume of C57 mice bearing LLC tumors and treated with different SLNs ($n = 10$). Mice treated with Pp-PTX-SLNs survived significantly longer than did mice that received Taxol® intravenously. $^{\#}p < 0.01$, $^{*}p < 0.05$, compared with Taxol®-treated group. Results shown are mean ± SD values.

(Abraxane®) in tumor tissues was only 1.33-fold higher than that of Taxol® (39), while the accumulation rate of Pp-PTX-SLNs was 4.35-fold higher than that of Taxol®. This reveals advantages of this nanoparticle approach over Abraxane®, the most recent clinically established PTX formulation designed to overcome the serious adverse effects of Taxol®. Furthermore, the tumor accumulation of our nanoparticles was also specific: the accumulation of Pp-PTX-SLNs in tumor tissue was significantly higher than that of Pp'-PTX-SLNs ($p<0.05$), indicating the importance of tumor-specific cleavage for activating the drug delivery system. Our finding that Pp-PTX-SLNs accumulated in heart, lung, and liver to a lesser extent than did Taxol® may reduce PTX toxicity in these tissues, which usually suffer the greatest toxic effects during PTX therapy. These findings strongly suggest that conjugating cleavable PEG-peptide to SLNs enhances tumor targeting and subsequent drug accumulation in tumor tissue.

To study the efficacy of our drug delivery system, we measured tumor growth (Fig. 7) and survival time (Fig. 8) in mice with LLC tumors treated with SLN formulations, Taxol® or saline. Log-rank analysis showed that Pp-PTX-SLNs led to significantly longer survival than did Pp'-PTX-SLNs ($p<0.05$), PTX-SLNs ($p<0.01$), Taxol® ($p<0.01$), and saline ($p<0.01^{\#}$). These differences in survival time can be attributed to the differences in accumulation of PTX in the tumor tissue. Compared with Pp'-PTX-SLNs, Pp-PTX-SLNs showed not only prolonged circulation but also enhanced accumulation at the tumor site because of the cleavable peptide linked to the PEG.

This PEG-peptide SLN drug delivery system offers a new strategy for paclitaxel chemotherapy and may be suitable for carrying other lipophilic chemotherapeutic drugs. Further studies should be conducted to optimize and confirm the tumor-targeting efficiency of this nanoparticle system. For

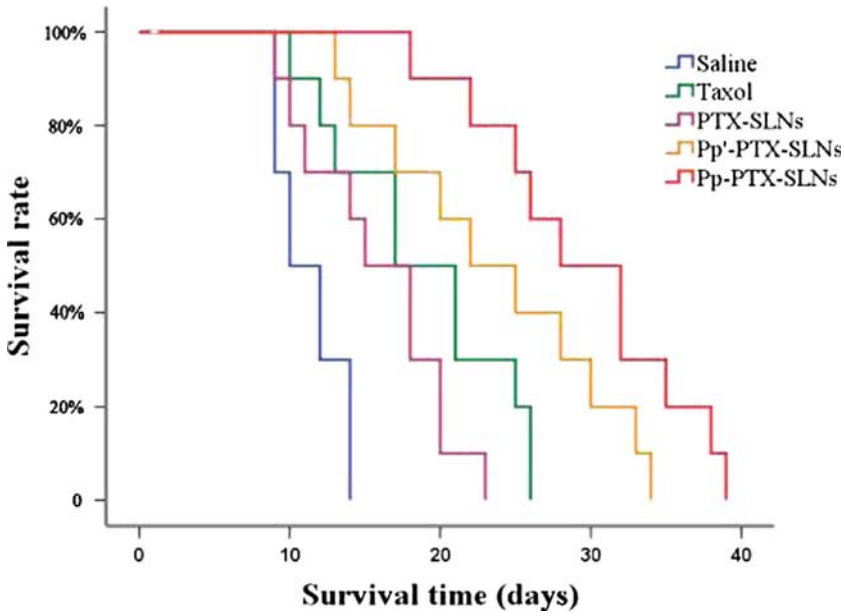

Fig. 8 Kaplan-Meier survival curves of mice bearing LLC tumors and treated with different SLNs ($n = 10$). Mice treated with Pp-PTX-SLNs survived significantly longer than did mice that received Pp'- PTX-SLNs ($p < 0.05$, log-rank analysis), Taxol® ($p < 0.01$), PTX-SLNs ($p < 0.01$) or saline ($p < 0.01$).

example, the molecular weight and structure of PEG (e.g., linear, branched and blocked (40)), which substantially influence nanoparticle properties, should be optimized to maximize efficacy and minimize toxicity. The balance between PEGylation and de-PEGylation should also be optimized to maximize the benefits of this drug delivery system.

CONCLUSION

PTX-loaded SLNs were successfully conjugated with PEG-matrix metalloproteinase (MMP)-substrate peptide. The PEG peptide was cleaved specifically by MMPs overexpressed in the tumor microenvironment, facilitating the uptake of the nanoparticles by tumor cells. Pp-PTX-SLNs accumulated to a greater extent in tumor tissue than did the non-cleavable Pp'-PTX-SLNs, leading to better efficacy in a mouse tumor model. Pp-PTX-SLNs also persisted much longer in the circulation than did non-PEGylated PTX-SLNs. Compared with Taxol®, Pp-PTX-SLNs showed lower distribution in heart, lung, and liver, suggesting that encapsulating PTX in SLNs may decrease the major side effects of PTX. The Pp-SLN delivery system may be suitable for other lipophilic chemotherapeutic drugs.

ACKNOWLEDGMENTS AND DISCLOSURES

Jie Zheng and Yu Wan contributed equally to this work. We are grateful for financial support from the University of Central Lancashire, the National Natural Science Foundation of China (No. 81173011) and the National Science & Technology Major Project of China (No. 2011ZX09401-304(4-3)).

REFERENCES

1. Rivkin I, Cohen K, Koffler J, Melikhov D, Peer D, Margalit R. Paclitaxel-clusters coated with hyaluronan as selective tumor-targeted nanovectors. Biomaterials. 2010;31(27):7106–14.
2. Guo W, Johnson JL, Khan S, Ahmad A, Ahmad I. Paclitaxel quantification in mouse plasma and tissues containing liposome-entrapped paclitaxel by liquid chromatography-tandem mass spectrometry: application to a pharmacokinetics study. Anal Biochem. 2005;336(2):213–20.
3. Konno T, Watanabe J, Ishihara K. Enhanced solubility of paclitaxel using water-soluble and biocompatible 2-methacryloyloxyethyl phosphorylcholine polymers. J Biomed Mater Res A. 2003;65(2):209–14.
4. Yoshizawa Y, Kono Y, Ogawara K, Kimura T, Higaki K. PEG liposomalization of paclitaxel improved its *in vivo* disposition and antitumor efficacy. Int J Pharm. 2011;412(1–2):132–41.
5. Yang T, Choi MK, Cui FD, Kim JS, Chung SJ, Shim CK, *et al.* Preparation and evaluation of paclitaxel-loaded PEGylated immunoliposome. J Control Release. 2007;120(3):169–77.
6. Hu FQ, Ren GF, Yuan H, Du YZ, Zeng S. Shell cross-linked stearic acid grafted chitosan oligosaccharide self-aggregated micelles for controlled release of paclitaxel. Colloids Surf B: Biointerfaces. 2006;50(2):97–103.
7. Rossi J, Giasson S, Khalid MN, Delmas P, Allen C, Leroux JC. Long-circulating poly(ethylene glycol)-coated emulsions to target solid tumors. Eur J Pharm Biopharm. 2007;67(2):329–38.
8. Li R, Eun JS, Lee MK. Pharmacokinetics and biodistribution of paclitaxel loaded in pegylated solid lipid nanoparticles after intravenous administration. Arch Pharm Res. 2011;34(2):331–7.
9. Caruthers SD, Wickline SA, Lanza GM. Nanotechnological applications in medicine. Curr Opin Biotechnol. 2007;18(1):26–30.
10. Kataoka K, Harada A, Nagasaki Y. Block copolymer micelles for drug delivery: design, characterization and biological significance. Adv Drug Deliv Rev. 2001;47(1):113–31.
11. Mishra S, Webster P, Davis ME. PEGylation significantly affects cellular uptake and intracellular trafficking of non-viral gene delivery particles. Eur J Cell Biol. 2004;83(3):97–111.
12. Xu H, Deng Y, Chen D, Hong W, Lu Y, Dong X. Esterase-catalyzed dePEGylation of pH-sensitive vesicles modified with cleavable PEG-lipid derivatives. J Control Release. 2008;130(3):238–45.
13. Terada T, Iwai M, Kawakami S, Yamashita F, Hashida M. Novel PEG-matrix metalloproteinase-2 cleavable peptide-lipid containing galactosylated liposomes for hepatocellular carcinoma-selective targeting. J Control Release. 2006;111(3):333–42.
14. Kurschat P, Zigrino P, Nischt R, Breitkopf K, Steurer P, Klein CE, *et al.* Tissue inhibitor of matrix metalloproteinase-2 regulates matrix metalloproteinase-2 activation by modulation of membrane-type 1 matrix metalloproteinase activity in high and low invasive melanoma cell lines. J Biol Chem. 1999;274(30):21056–62.
15. Mansour AM, Drevs J, Esser N, Hamada FM, Badary OA, Unger C, *et al.* A new approach for the treatment of malignant melanoma: enhanced antitumor efficacy of an albumin-binding doxorubicin prodrug that is cleaved by matrix metalloproteinase 2. Cancer Res. 2003;63(14):4062–6.
16. Wan Y, Han J, Fan G, Zhang Z, Gong T, Sun X. Enzyme-responsive liposomes modified adenoviral vectors for enhanced tumor cell transduction and reduced immunogenicity. Biomaterials. 2013;34(12):3020–30.
17. Nikanjam M, Gibbs AR, Hunt CA, Budinger TF, Forte TM. Synthetic nano-LDL with paclitaxel oleate as a targeted drug delivery vehicle for glioblastoma multiforme. J Control Release. 2007;124(3):163–71.
18. Shimada K, Matsuo S, Sadzuka Y, Miyagishima A, Nozawa Y, Hirota S, *et al.* Determination of incorporated amounts of poly(ethylene glycol)-derivatized lipids in liposomes for the physicochemical characterization of stealth liposomes. Int J Pharm. 2000;203(1–2):255–63.
19. Zeng N, Hu Q, Liu Z, Gao X, Hu R, Song Q, *et al.* Preparation and characterization of paclitaxel-loaded DSPE-PEG-liquid crystalline nanoparticles (LCNPs) for improved bioavailability. Int J Pharm. 2012;424(1–2):58–66.
20. Elliott P, Hohmann A, Spanos J. Protease expression in the supernatant of Chinese hamster ovary cells grown in serum-free culture. Biotechnol Lett. 2003;25(22):1949–52.
21. Goutayer M, Dufort S, Josserand V, Royere A, Heinrich E, Vinet F, *et al.* Tumor targeting of functionalized lipid nanoparticles: assessment by *in vivo* fluorescence imaging. Eur J Pharm Biopharm. 2010;75(2):137–47.
22. Chambers AF, Matrisian LM. Changing views of the role of matrix metalloproteinases in metastasis. J Natl Cancer Inst. 1997;89(17):1260–70.
23. Li SD, Huang L. Stealth nanoparticles: high density but sheddable PEG is a key for tumor targeting. J Control Release. 2010;145(3):178–81.
24. Skubitz KM. Phase II, trial of pegylated-liposomal doxorubicin (Doxil) in sarcoma. Cancer Investig. 2003;21(2):167–76.
25. Kirpotin D, Hong K, Mullah N, Papahadjopoulos D, Zalipsky S. Liposomes with detachable polymer coating: destabilization and fusion of dioleoylphosphatidylethanolamine vesicles triggered by

cleavage of surface-grafted poly(ethylene glycol). FEBS Lett. 1996;388(2–3):115–8.
26. Andreu D, Albericio F, Solé NA, Munson MC, Ferrer M, Barany G. Formation of disulfide bonds in synthetic peptides and proteins. Methods Mol Biol. 1994;35:91–169.
27. Drummond DC, Zignani M, Leroux J. Current status of pH-sensitive liposomes in drug delivery. Prog Lipid Res. 2000;39(5):409–60.
28. Jackson CJ, Arkell J, Nguyen M. Rheumatoid synovial endothelial cells secrete decreased levels of tissue inhibitor of MMP (TIMP1). Ann Rheum Dis. 1998;57(3):158–61.
29. Sato H, Takino T, Okada Y, Cao J, Shinagawa A, Yamamoto E, *et al.* A matrix metalloproteinase expressed on the surface of invasive tumour cells. Nature. 1994;370(6484):61–5.
30. Allen C, Dos Santos N, Gallagher R, Chiu GN, Shu Y, Li WM, *et al.* Controlling the physical behavior and biological performance of liposome formulations through use of surface grafted poly(ethylene glycol). Biosci Rep. 2002;22(2):225–50.
31. Fang C, Shi B, Pei YY, Hong MH, Wu J, Chen HZ. *In vivo* tumor targeting of tumor necrosis factor-alpha-loaded stealth nanoparticles: effect of MePEG molecular weight and particle size. Eur J Pharm Sci. 2006;27(1):27–36.
32. Kohane DS. Microparticles and nanoparticles for drug delivery. Biotechnol Bioeng. 2007;96(2):203–9.
33. Xiao K, Luo J, Fowler WL, Li Y, Lee JS, Xing L, *et al.* A self-assembling nanoparticle for paclitaxel delivery in ovarian cancer. Biomaterials. 2009;30(30):6006–16.
34. Martins S, Costa-Lima S, Carneiro T, Cordeiro-da-Silva A, Souto EB, Ferreira DC. Solid lipid nanoparticles as intracellular drug transporters: an investigation of the uptake mechanism and pathway. Int J Pharm. 2012;430(1–2):216–27.
35. Xu Z, Gu W, Huang J, Sui H, Zhou Z, Yang Y, *et al. In vitro* and *in vivo* evaluation of actively targetable nanoparticles for paclitaxel delivery. Int J Pharm. 2005;288(2):361–8.
36. Chen DB, Yang TZ, Lu WL, Zhang Q. *In vitro* and *in vivo* study of two types of long-circulating solid lipid nanoparticles containing paclitaxel. Chem Pharm Bull. 2001;49(11):1444–7.
37. Li X, Cheng X, Wang Y, Mao L, Wang Y, Huang Q. Preparation of Paclitaxel Nanosuspension and Study of Its Pharmacokinetic and Biodistrabution Behavior in Rats. Chin Pharm J. 2011;9:015.
38. Zhang Z, Lee SH, Gan CW, Feng SS. *In vitro* and *in vivo* investigation on PLA-TPGS nanoparticles for controlled and sustained small molecule chemotherapy. Pharm Res. 2008;25(8):1925–35.
39. Desai N, Trieu V, Yao Z, Louie L, Ci S, Yang A, *et al.* Increased antitumor activity, intratumor paclitaxel concentrations, and endothelial cell transport of cremophor-free, albumin-bound paclitaxel, ABI-007, compared with cremophor-based paclitaxel. Clin Cancer Res Off J Am Assoc Cancer Res. 2006;12(4):1317–24.
40. Park K. To PEGylate or not to PEGylate, that is not the question. J Control Release. 2010;142(2):147–8.